Article

Computational Analysis of MHD Nonlinear Radiation Casson Hybrid Nanofluid Flow at Vertical Stretching Sheet

Nadeem Abbas [1], Wasfi Shatanawi [1,2,3,*] and Kamaleldin Abodayeh [1]

1   Department of Mathematics and Sciences, College of Humanities and Sciences,
    Prince Sultan University, Riyadh 11586, Saudi Arabia; nabbas@psu.edu.sa (N.A.); kamal@psu.edu.sa (K.A.)
2   Department of Medical Research,
    China Medical University Hospital, China Medical University, Taichung 40402, Taiwan
3   Department of Mathematics, Faculty of Science, The Hashemite University, Zarqa 13133, Jordan
*   Correspondence: wshatanawi@psu.edu.sa

Abstract: The stagnation point flow of unsteady compressible Casson hybrid nanofluid flow over a vertical stretching sheet was analyzed. The comparative study of Yamada Ota, Tiwari Das, and Xue hybrid nanofluid models was performed. The Lorentz force was applied normal to flow directions. The effect of nonlinear radiation was studied. We considered the SWCNT (signal wall carbon nanotube) and MWCNT (multi-wall carbon nanotube) with base liquid (water). Under the flow suppositions, a mathematical model was settled by means of boundary layer approximations in terms of partial differential equations. The suitable transformation was developed by using the lie symmetry method. Partial differential equations were transformed into ordinary differential equations by suitable transformations. The dimensionless system was elucidated through a numerical technique named bvp4c. The impacts of pertinent flow parameters on skin friction, Nusselt number, and temperature and velocity distributions were depicted through tabular form as well as graphical form. In this study, the Yamada Ota model achieved a higher heat transfer rate compared to the Tiwari Das and Xue hybrid nanofluid models. The skin friction ($C_{fx}Re^{-1/2}$) increased and temperature gradient ($Nu_xRe^{-1/2}$) declined due to the increment of solid nanoparticle concentration (ϕ_2). Physically, skin friction increased because the higher values of the solid nanoparticles increased resistance to the fluid motion.

Keywords: Casson hybrid nanofluid; nonlinear radiation; MHD; thermal slip; viscous dissipation

1. Introduction

A new generation of nanofluids has been studied extensively; these liquids are referred to as hybrid nanofluids. Due to their combined action on multiple nano-elements with base fluid, hybrid nanofluids have developed thermal properties. Due to several positive advantages over nanofluids, this latest development, which was caused by the addition of various nanoparticles in the working liquid, has become a popular topic among scientists. A hybrid nanofluid is a mixture of two solid nanoparticles and based fluids. The base fluid (ordinary fluid) has less thermal conductivity and low heat transfer phenomena exist. Additions of solid nanoparticles in the base fluid (ordinary fluid) increased the heat transfer rate due to increment physical characteristics because the thermal conductivity of the liquid is lesser than solid nanoparticles. In the beginning, the word nanofluid was initiated by Choi and Eastman [1]. They assembled the mixture of nanosized solid particles with ordinary fluid (base fluid). This imitative work is much attracted due to the increment of heat transfer phonemes exist. Reddy et al. [2] highlighted the impacts of the chemical reaction and thermal radiation with base fluid Casson nanofluid at a stretching surface. They presented their work numerically under the influence of source and sink. Vajravelu et al. [3] discussed the comparative analysis of nanofluid using the different nanoparticles namely silver and copper with base ordinary fluid (water) at a stretching surface. Furthermore, energy crises are one of the most problems in the world. Every researcher developed the

models which improved the heat transfer phenomena at less cost. New develop a model of modified nanofluid in these problems namely hybrid nanofluid. The hybrid nanofluid is a mixture of two solid nanoparticles and base fluid (ordinary liquid). This invention of hybrid nanofluid attracted the investigators to provide the area of research in different flow assumptions. Suresh et al. [4] proposed the model of hybrid nanofluid flow and achieved the results experimentally. They considered two solid nanosized particles namely: copper and aluminium oxide with base fluid (liquid water). They highlighted the results and achieved a heat transfer rate of more than twice as compared to simple ordinary fluid. Suresh et al. [5] implemented the hybrid nanofluid model for boundary layer flow. They get the results of heat transfer rate well twice times as compared to simple ordinary fluid. Takabi and Shokouhmand [6] discussed the hybrid nanofluid effects on turbulent regimes. Nadeem et al. [7] initiated the results of hybrid nanofluid flow at a stretching cylinder. They worked for stagnation flow with MHD and slip effects. Nadeem and Abbas [8] studied the influences of hybrid nanofluid at stretching cylinder. They also considered the micropolar fluid model with slip and MHD effects. They also discussed the impacts of stagnation regions with weak and strong concentration. Nadeem et al. [9] indicated the impacts of hybrid nanofluid flow at stretching curved surfaces. They considered the SWCNT and MWCNT with base fluid (ordinary fluid). The thermal slip is considered in their analysis. Abbas et al. [10] considered the inclined magnetic hydrodynamics flow of hybrid nanofluid at a stretching cylinder. They extended the Yamada Ota and Xue model in terms of hybrid nanofluid. They achieved the results of Yamada Ota model of hybrid nanofluid with more heat transfer rate as compared to the Xue model of hybrid nanofluid. Abbas et al. [11] investigated the numerical results of hybrid nanofluid flow at the permeable stretching curved surface. In recent days, several researchers developed the heat transfer phenomena for different assumptions of fluid flow see Refs. [12,13].

Casson fluid model is one of the classes of non-Newtonian fluid which defined the properties of yield stress. Casson fluid is commonly used in real-life namely: in jelly, honey, sauce, concentrated fruit juices, and soup, etc. Furthermore, its wide applications in the fields of industries which improved day by day. The study of the non-Newtonian fluid is much more difficult dynamically as well as complex nature and interactions. Casson fluid lies in the type of dilatant fluids because it has zero shear stress at infinity viscosity. If the yield stress is greater than applied stress than fluid behavior like solid but yield stress is lesser than applied stress than fluid behavior like to liquid move. Casson [14] initiated the equation of the Casson fluid model. This model was developed and many researchers were attracted to solve the problem. Abbas and Shatanawi [15] scrutinized the casson nanofluid flow at the stretching sheet. Nadeem et al. [16] highlighted the influence of magnetic hydrodynamics of Casson nanofluid with convective boundary conditions. They also discussed the Brownian motion and thermophoresis influence. Oyelakin et al. [17] explored the time-dependent flow of Casson fluid flow at a stretching sheet. They studied the effects of thermal radiation, slip and convective boundary conditions. They also depicted the influences of Brownian motion and thermophoresis. Ibrahim et al. [18] investigated the mixed convection of Casson nanofluid with MHD and viscous dissipation. They achieved the numerical results with impacts of heat source and chemical reaction. Amjad et al. [19] considered the Casson micropolar fluid flow at a curved surface. They discussed the induced magnetic hydrodynamics with Brownian and thermophoresis motion. Lanjwani et al. [20] scrutinized triple solutions of Casson nanofluid at the vertical nonlinear stretching sheet. Several authors studied the influence of various physical parameters under flow assumption see Refs. [21–23].

Little attention to unsteady flow over-stretching sheets is one of the most important topics developed in the literature. Yang [24] initiated the idea of unsteady flow under the stagnation region. He solved the Navier–Stokes equations and achieved the results in a closed-form solution. Furthermore, Wang [25] extended the idea of Yang [24] on the fluid film. He reduced the Navier–Stokes equations into nonlinear ordinary differential equations. The reduced system is solved numerically and asymptotically. These results

are near to the closed-form solutions. Abbas et al. [26] indicated the influence of non-Newtonian liquid at stretching surface. They implemented the HAM technique using the Mathematica software packages. Mabood and Shateyi [27] investigated the effects of time depending on MHD flow at a permeable stretching sheet. They considered the impacts of nonlinear radiation and multiple slips and implemented the numerical technique to solve the problem. Fuzhang et al. [28] studied the unsteady flow of non-Newtonian fluid at stretching curved surfaces. Recently, some authors developed the ideas to investigate the unsteady flow due to various assumptions see Refs. [29,30].

In this study, we considered the stagnation point unsteady flow of Casson hybrid nanofluid flow at the vertical stretching sheet. The Lorentz force is applied normal to flow directions. The effects of the nonlinear radiation are studied. Three types of hybrid nanofluid models are investigated in the current analysis. The SWCNT and MWCNT with base fluid water are considered. Under the above suppositions, a mathematical model is constructed in differential equations (Partial Differential Equations) utilizing BLA (Boundary Layer Approximations). Thermal and velocity slip impacts are analyzed. From the above assumptions, the coupled nonlinear PDEs transformed into nonlinear coupled ODEs using the set of suitable transformations. The nonlinear coupled ODEs are solved through numerical technique along the Runge-Kutta scheme. The MHD stagnation point flow of unsteady Casson hybrid nanofluid with nonlinear radiation over vertical stretching sheet is not discussed using three models of hybrid nanofluids namely: Yamada Ota model, Tiwari Das model and Xue model under the thermal sip. The influence of dimensionless physical parameters is presented through graphs and tables.

2. Materials and Methods

Two-dimensional unsteady flow of incompressible stagnation point flow of Casson hybrid nanofluid over vertical stretching sheet is considered which is seen in Figure 1. Two slid different nanoparticles (SWCNT and MWCNT) with base fluid (H_2O) are used to analyze the comparative results of Yamada and Ota [31], Xue [32] and Tiwari and Das [33] for hybrid nanofluid. The constant wall temperature (T_w) is stretched along the vertical direction as $y \to 0$. The ambient temperature is for away from the stretching sheet as $y \to \infty$. The B_0 is induced to stretched sheet in normal direction as a transverse uniform magnetic field. Moreover, the induced magnetic field is considered negligible in comparison to the applied magnetic field because the magnetic Reynold number is very small. The influence of thermal radiation is considered in the thermal boundary layer equation. The main assumptions of the governing equations are presented below:

- Unsteady flow of Casson hybrid nanofluid
- Stagnation point flow
- Thermal slip and nonlinear radiation
- MHD
- Vertical stretching sheet

Using the above assumptions, the mathematical model is developed using the boundary layer approximations in terms of partial differential equations. The system of differential equations is presented below (see Refs. [9–11]).

$$\frac{\partial u}{\partial x} + \frac{\partial v}{\partial y} = 0,　\tag{1}$$

$$\frac{\partial u}{\partial t} + u\frac{\partial u}{\partial x} + v\frac{\partial u}{\partial y} = u_e\frac{\partial u_e}{\partial x} + \nu_{hnf}\left(1 + \frac{1}{\beta}\right)\frac{\partial^2 u}{\partial y^2} - \frac{\sigma_e B_0{}^2}{\rho_{hnf}}(u - u_e) + g\frac{(\beta_T)_{hnf}}{\rho_{hnf}}(T - T_\infty),　\tag{2}$$

$$\frac{\partial T}{\partial t} + u\frac{\partial T}{\partial x} + v\frac{\partial T}{\partial y} = \alpha_{hnf}\frac{\partial T}{\partial y^2} + \frac{\sigma_e B_0{}^2}{\left(\rho c_P\right)_{hnf}}(u_e - u)^2 - \frac{1}{(\rho c)_{hnf}}\frac{\partial q_r}{\partial y}.　\tag{3}$$

Having the boundary conditions are

$$u = 0, \ v = 0, \ T = T_w + \gamma_2 \frac{k^*_{hnf}}{k^*_f} \frac{\partial T}{\partial y}, \ \text{as } y \to 0, \\ u = u_e, \ T = T_\infty \text{ as } y \to \infty. \tag{4}$$

The suitable transformations are introduced,

$$u_e = \frac{ax}{\sqrt{1-\alpha t}}, \quad \eta = \sqrt{\frac{a}{v_f (1-\alpha t)}} y, \quad u = \frac{ax}{1-\alpha t} F'(\eta), \\ v = -\sqrt{\frac{a \, v_f}{1-\alpha t}} F(\eta), \quad \theta(\eta) = \frac{T-T_\infty}{T_w-T_\infty}, \quad q_r = -\frac{16 \, \sigma \, T^3}{3} \frac{\partial T}{\partial y}. \tag{5}$$

The suitable transformations are implemented on the above differential equations which are as following:

$$\left(\frac{1}{A} + \frac{1}{\beta} \right) \left(\frac{1}{B} \right) F'''(\eta) + 1 - \left(\frac{\delta}{B} \right) \left(F'(\eta) - 1 \right) + F''(\eta) F(\eta) - \left(F'(\eta) \right)^2 - \frac{\alpha}{2B} \left(F'(\eta) - \eta \, F''(\eta) \right) + \left(\frac{\tau}{B} \right) \theta(\eta) = 0, \tag{6}$$

$$\frac{k^*_{hnf}}{Pr k^*_f \, C} \left(1 + \frac{4}{3} R_d \right) \theta''(\eta) + F(\eta) \, \theta'(\eta) + \frac{A\alpha}{2C} \eta \, \theta'(\eta) + \frac{\delta}{C} \left(F'(\eta) - 1 \right) \left(F'(\eta) - 1 \right) = 0, \tag{7}$$

concerning the boundary conditions are:

$$F(0) = 0, \ F'(0) = 0, \ F'(\infty) = 1, \ \theta(0) = 1 + \frac{k^*_{hnf}}{k^*_f} \lambda \, \theta'(0), \ \theta(\infty) = 0. \tag{8}$$

where, $A = ((1+\phi_2)(1+\phi_1))^{2.5}$, $B = \left((1-\phi_2)(1-\phi_1) + \phi_2 \left(\frac{\rho_{s_2}}{\rho_f} \right) + \phi_1 \left(\frac{\rho_{s_1}}{\rho_f} \right) \right)$ and $C = \left((1-\phi_2)(1-\phi_1) + \phi_1 \left(\frac{(\rho c_p)_{s_1}}{(\rho c_p)_f} \right) + \phi_2 \left(\frac{(\rho c_p)_{s_2}}{(\rho c_p)_f} \right) \right)$.

The nanofluid models were proposed by Yamada and Ota [31] and Xue [32]. Tiwari and Das [33] proposed hybrid nanofluid model. The Yamada and Ota [31] and Xue [32] of nanofluid were extended by Abbas et al. [34] and Abbas et al. [35]. They considered the two solid nanoparticles in this analysis. The models of hybrid nanofluid were introduced. The expression of the Yamada-Ota model is presented below:

$$\frac{k^*_{bf}}{k^*_f} = \frac{1 + \frac{k^*_f}{k^*_{s_1}} \frac{L}{R} \phi_1^{0.2} + \left(1 - \frac{k^*_f}{k^*_{s_1}} \right) \phi_1 \frac{L}{R} \phi_1^{0.2} + 2\phi_1 \left(\frac{k^*_{s_1}}{k^*_{s_1} - k^*_f} \right) \ln \left(\frac{k^*_{s_1} + k^*_f}{2k^*_{s_1}} \right)}{1 - \phi_1 + 2\phi_1 \left(\frac{k^*_f}{k^*_{s_1} - k^*_f} \right) \ln \left(\frac{k^*_{s_1} + k^*_f}{2k^*_f} \right)},$$

$$\frac{k^*_{hnf}}{k^*_{bf}} = \frac{1 + \frac{k^*_{bf}}{k^*_{s_2}} \frac{L}{R} \phi_2^{0.2} + \left(1 - \frac{k^*_{bf}}{k^*_{s_2}} \right) \phi_2 \frac{L}{R} \phi_2^{0.2} + 2\phi_2 \left(\frac{k^*_{s_2}}{k^*_{s_2} - k^*_{bf}} \right) \ln \left(\frac{k^*_{s_2} + k^*_{bf}}{2k^*_{s_2}} \right)}{1 - \phi_2 + 2\phi_2 \left(\frac{k^*_{bf}}{k^*_{s_2} - k^*_{bf}} \right) \ln \left(\frac{k^*_{s_2} + k^*_{bf}}{2k^*_{bf}} \right)},$$

The expression of the Xue model is presented below:

$$\frac{k^*_{bf}}{k^*_f} = \frac{1 - \phi_1 + 2\phi_1 \left(\frac{k^*_{s_1}}{k^*_{s_1} - k^*_f} \right) \ln \left(\frac{k^*_{s_1} + k^*_f}{2k^*_f} \right)}{1 - \phi_1 + 2\phi_1 \left(\frac{k^*_f}{k^*_{s_1} - k^*_f} \right) \ln \left(\frac{k^*_{s_1} + k^*_f}{2k^*_f} \right)},$$

$$\frac{k^*_{hnf}}{k^*_{bf}} = \frac{1 - \phi_2 + 2\phi_2 \left(\frac{k^*_{s_2}}{k^*_{s_2} - k^*_{bf}} \right) \ln \left(\frac{k^*_{s_2} + k^*_{bf}}{2k^*_{bf}} \right)}{1 - \phi_2 + 2\phi_2 \left(\frac{k^*_{bf}}{k^*_{s_2} - k^*_{bf}} \right) \ln \left(\frac{k^*_{s_2} + k^*_{bf}}{2k^*_{bf}} \right)}.$$

The expression of the Tiwari-Das model is presented below:

$$\frac{k^*_{bf}}{k^*_f} = \frac{(n-1)k^*_f - \left(k^*_f - k^*_{s_1}\right)\phi_1(n-1) + k^*_{s_1}}{\left(k^*_f - k^*_{s_1}\right)\phi_1 + (n-1)k^*_f + k^*_{s_1}},$$

$$\frac{k^*_{hnf}}{k^*_{bf}} = \frac{(n-1)k^*_{bf} - \left(k^*_{bf} - k^*_{s_2}\right)\phi_2(n-1) + k^*_{s_2}}{\left(k^*_{bf} - k^*_{s_2}\right)\phi_2 + (n-1)k^*_{bf} + k^*_{s_2}}.$$

The physical properties are defined as below (see Refs. [34,35]):

Thermophysical properties	MWCNT	SWCNT	H_2O
$\rho\left(Jkg^{-1}K^{-1}\right)$	1600	2600	997.1
$k^*\left(kgm^{-3}\right)$	3000	6600	0.613
$c_p\left(Wm^{-1}K^{-1}\right)$	796	425	4179

Solution Procedure

The system of differential equations is a nonlinear boundary value problem. There are several methods that have been applied to solve the nonlinear boundary value problem arising in the fluid dynamics (see Refs. [36,37]). The system of nonlinear higher-order differential Equations (6) and (7) subject to boundary conditions (8) is solved through the Runge-Kutta-Fehlberg scheme (shooting method). The higher-order nonlinear differential equations are transformed into first-order differential equations. The procedure is defined as follows:

$$F(\eta) = y(1); \tag{9}$$

$$F'(y) = y(2); \tag{10}$$

$$F''(y) = y(3); \tag{11}$$

$$F'''(y) = yy1; \tag{12}$$

$$yy_1 = -\left(\left(\frac{1}{A} + \frac{1}{\beta}\right)^{-1}\right)B\begin{pmatrix} y(1)\,y(3) + 1 - y(2)y(2) + \left(\frac{\alpha}{2}B\right) \\ (x\,y(3) - y(2)) \\ -\left(\frac{\delta}{B}\right)(y(2) - 1) + \frac{\tau}{B}y(4) \end{pmatrix}, \tag{13}$$

$$\theta(\eta) = y(4); \tag{14}$$

$$\theta'(\eta) = y(5); \tag{15}$$

$$\theta''(\eta) = yy2; \tag{16}$$

$$yy_2 = -\left(\left(\frac{Prk^*_f}{k^*_{hnf}}\right)\left(\frac{C}{\left(1 + \frac{4}{3}R_d\right)}\right)\right)\left(y(5)\,y(1) + \left(\frac{\alpha}{2}\right)x\,y(5) + \left(\frac{\delta}{C}\right)\left((y(2) - 1)^2\right)\right). \tag{17}$$

With relevant boundary conditions are

$$y_0(1);\ y_0(2);\ y_{inf}(2) - 1;\ y_0(4) - 1 - \frac{k^*_{hnf}}{k^*_f}\lambda y_0(5);\ y_{inf}(4); \tag{18}$$

The nonlinear higher-order differential system is solved by using the fifth-order Runge-Kutta-Fehlberg scheme. The average time of the CPU is 16.8765 s. The numerical results will convergence if the boundary residuals $(R_1(u_1, u_2), R_2(u_1, u_2))$ are less than tolerance error i.e., 10^{-6}. Something else, introductory approximations are altered with the Newton

method and the method is repeated unless it meets the required convergence basis. The boundary residuals are presented as:

$$R_1(u_1, u_2) = |y_2(\infty) - \hat{y}_2(\infty)|,$$
$$R_2(u_1, u_2) = |y_4(\infty) - \hat{y}_4(\infty)|.$$

Hence, $\hat{y}_2(\infty)$ and $\hat{y}_4(\infty)$ are computed boundary values. The residuals of velocity and temperature are plotted in Figures 2 and 3. It turns out that 40 iterations are sufficient to achieve the desired accuracy of the calculated solution.
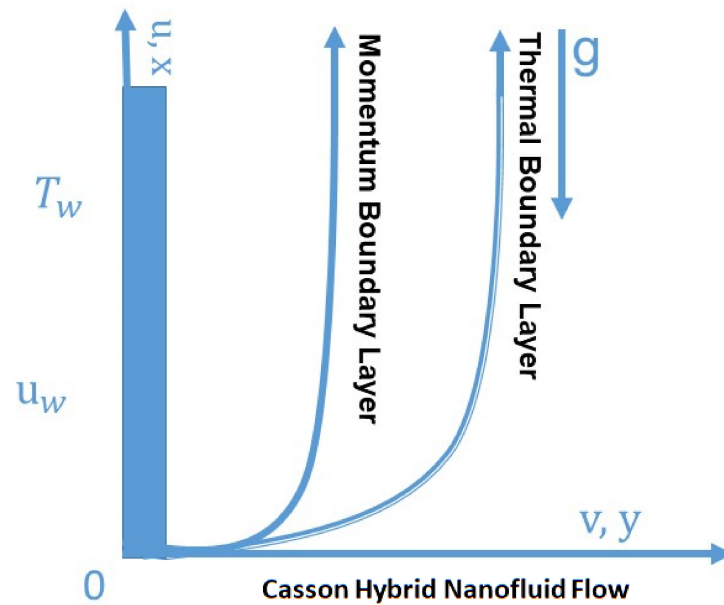

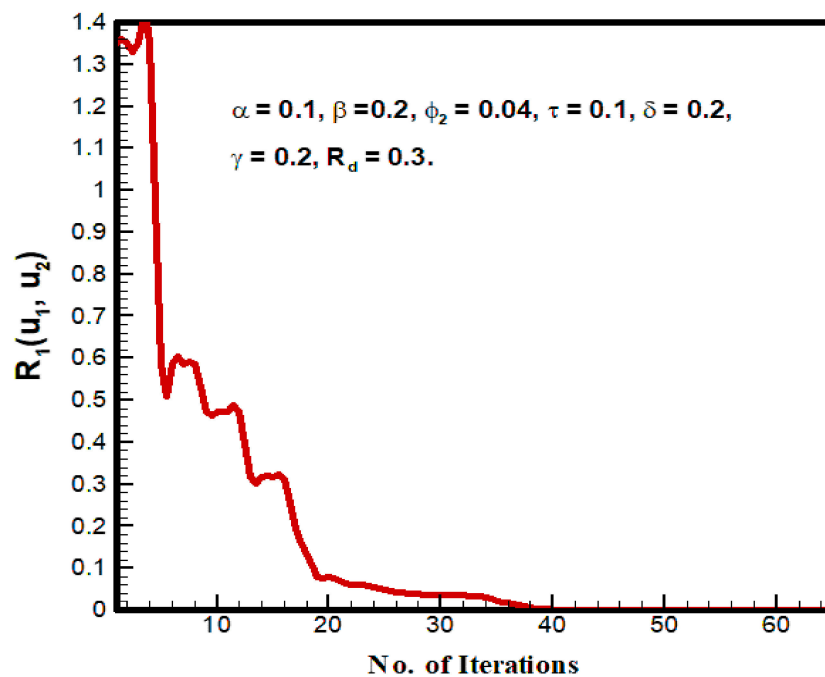**Figure 1.** The flow pattern of Casson hybrid nanofluid at the vertical sheet.
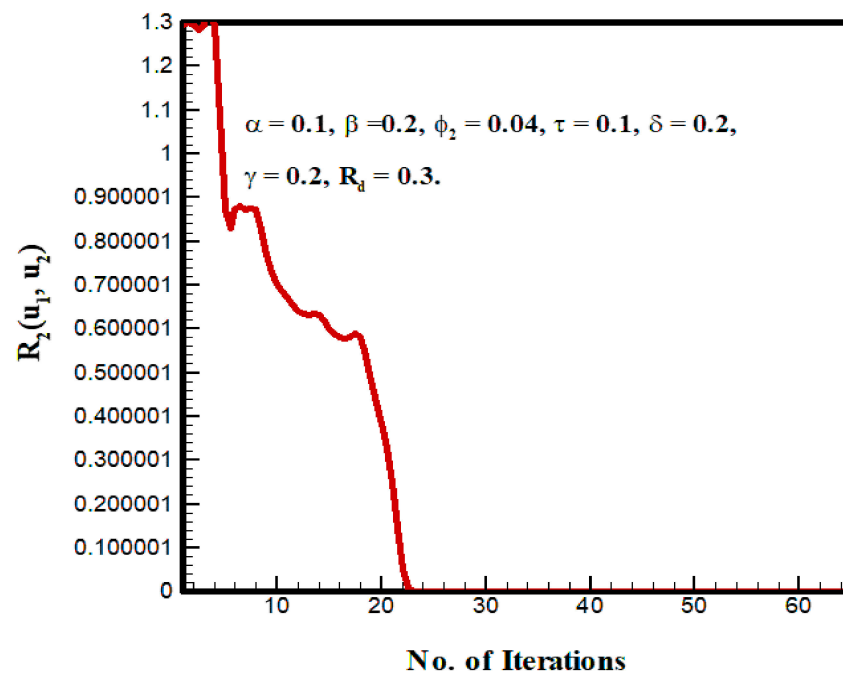

Figure 2. Residual $R_1(u_1, u_2)$.

Figure 3. Residual $R_2(u_1, u_2)$.

3. Results and Discussion

The impacts of physical parameters namely: unsteadiness parameter (α), solid nanoparticle concentration (ϕ_2), Casson fluid parameter (β), magnetic field parameter (δ), nonlinear radiation parameter (R_d), bouncy force parameter (τ) and thermal slip (λ) on the temperature function ($\theta(\eta)$), velocity function ($F'(\eta)$), Nusselt number ($Nu_x Re^{-1/2}$) and skin friction ($C_{fx} Re^{-1/2}$) presented through graphs and tabular form. Figures 4–7. indicated the impacts of solid nanoparticle concentration (ϕ_2), Casson fluid parameter (β), unsteadiness parameter (α) and magnetic field parameter (δ) on the velocity function ($F'(\eta)$). The variation of velocity function ($F'(\eta)$) and solid nanoparticle concentration (ϕ_2) are indicated in Figure 4. The curves of the velocity function revealed declining behaviour due to higher values of solid nanoparticle concentration (ϕ_2). Because higher values of the solid nanoparticles, which are increased resistance to the fluid motion, result in improved effective viscosity of hybrid nanoparticles with base fluid which declined the velocity of the fluid. Figure 5 indicated the influence of Casson fluid parameter (β) on the velocity function ($F'(\eta)$). The behaviour of velocity function ($F'(\eta)$) and Casson fluid parameter (β) were found to be the same increasing. The elasticity of the parameter is due to the relationship between relaxation and delay time. As the Casson parameter increases, the flow profile increases, indicating that the thickness of the lower confinement surface stops at zero. In fact, the higher the Casson value, the higher the primary velocity for the Newton case. Figure 6 revealed the variation of velocity function ($F'(\eta)$) and unsteadiness parameter (α). The curves of velocity function ($F'(\eta)$) revealed the declining behaviour due to the increment of the unsteadiness parameter (α). As the numerical contribution to the unsteadiness parameter increases, the thickness of the boundary layer associated with the velocity gradient decreases in both conditions. The unsteadiness parameter depends on buoyancy and the influence of buoyancy is strong, so the flow is upward and the velocity field of the liquid flow is reduced. The impacts of the magnetic field parameter (δ) on the velocity function ($F'(\eta)$) are revealed in Figure 7. The values of magnetic field (δ) increased which enhanced the curves of velocity function ($F'(\eta)$). Physically, when a magnetic field is applied to the boundary layer, Lorentz force is generated, and the Lorentz force is strengthened to increase the strength of the magnetic field. This force has a flow and increases the shear stress on the surface, resulting in an increase in thermal velocity. It should be noted

that the results of this study are inconsistent with those physical phenomena due to the interaction between the magnetic field and the flow discontinuity. The impacts of Casson fluid parameter (β), thermal slip (λ), unsteadiness parameter (α), magnetic field parameter (δ), nonlinear radiation parameter (R_d) and solid nanoparticle concentration (ϕ_2) on the temperature function ($\theta(\eta)$) which is indicated in Figures 8–13. Figure 8 highlighted the influence of Casson fluid parameter (β) on the temperature function ($\theta(\eta)$). The curves of the temperature function ($\theta(\eta)$) revealed declining due to improving the value of Casson fluid parameter (β). It is observed that as Casson fluid parameter (β) increases, the thermal boundary layer thickness decreases. Figure 9 highlighted the influence of thermal slip (λ) on the temperature function ($\theta(\eta)$). The curves of the temperature function ($\theta(\eta)$) revealed declining due to improving the value of thermal slip (λ). Physically, the increment in thermal slip declined the surface drag leading to a decline in the production of heat amount which reduced the temperature distribution. Figure 10 highlighted the influence of the unsteadiness parameter (α) on the temperature function ($\theta(\eta)$). The curves of the temperature function ($\theta(\eta)$) revealed declining due to improving the value of the unsteadiness parameter (α). The impacts of the magnetic field parameter (δ) on the temperature function ($\theta(\eta)$) are revealed in Figure 11. The values of magnetic field (δ) increased which enhanced the curves of temperature function ($\theta(\eta)$). The impacts of nonlinear radiation parameter (R_d) on the temperature function ($\theta(\eta)$) are revealed in Figure 12. The values of the nonlinear radiation parameter (R_d) increased which enhanced the curves of temperature function ($\theta(\eta)$). The impacts of solid nanoparticle concentration (ϕ_2) on the temperature function ($\theta(\eta)$) are revealed in Figure 13. The values of solid nanoparticle concentration (ϕ_2) increased which enhanced the curves of temperature function ($\theta(\eta)$). Physically, the thermal conductivity of the fluid enhanced which enhanced the heat transfer rate.
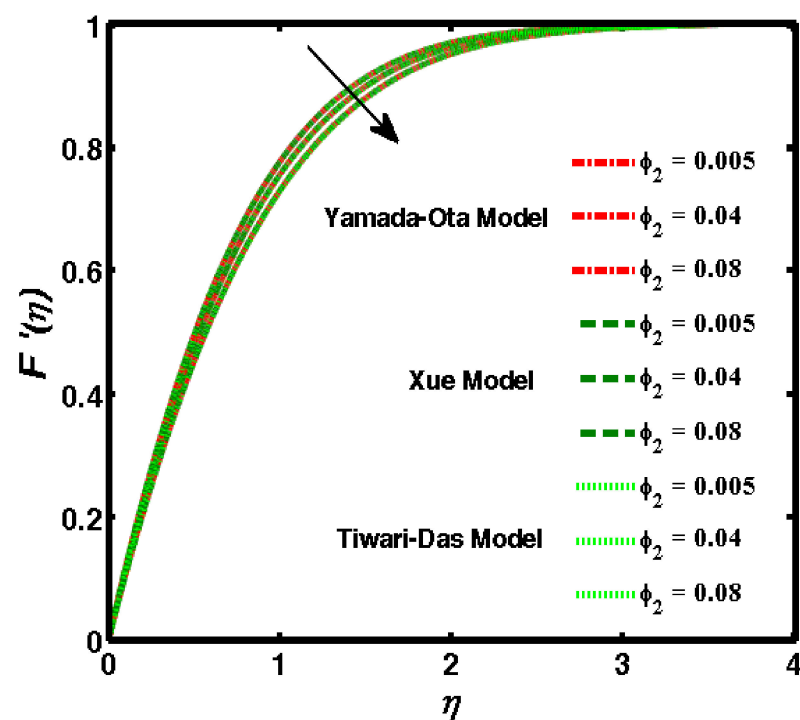

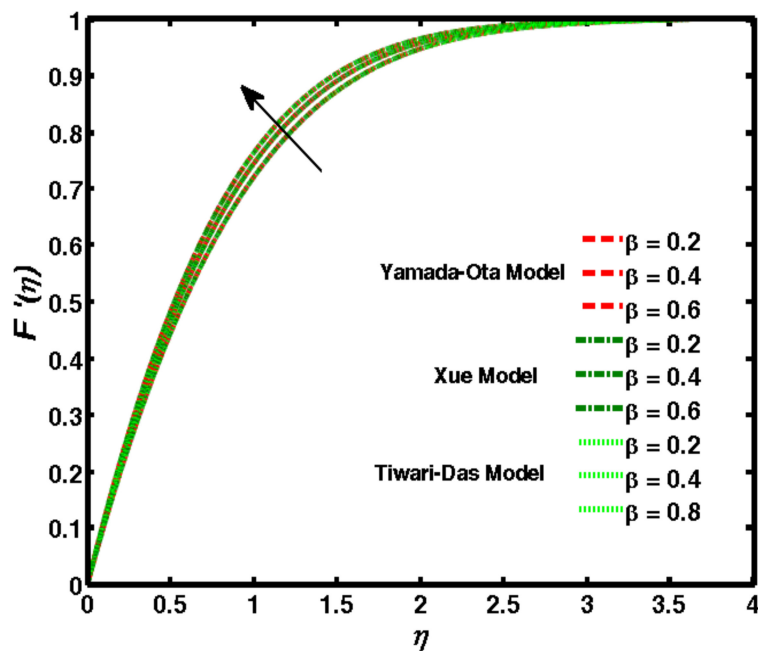**Figure 4.** Impacts of solid nanoparticle concentration on the velocity profile.

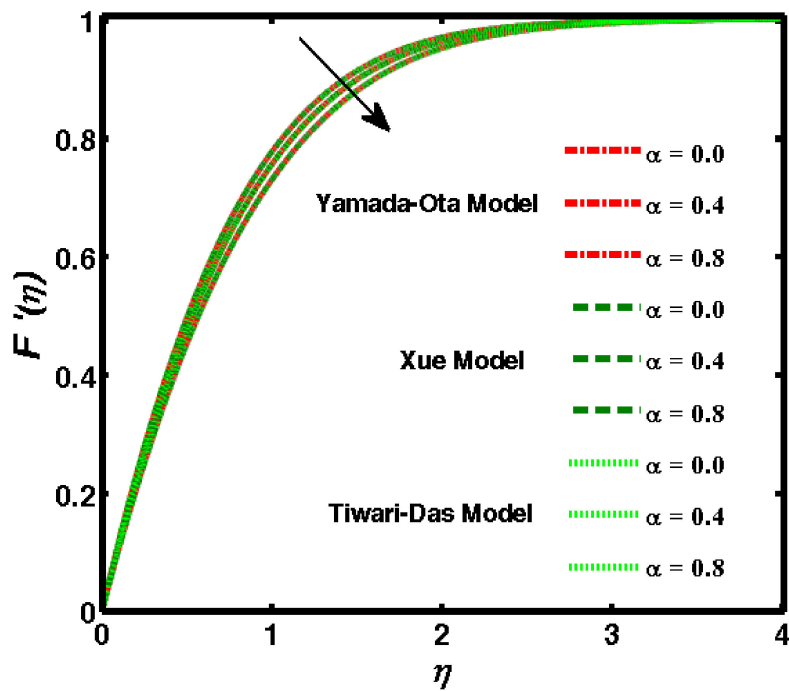**Figure 5.** Impacts of Casson fluid parameter on the velocity profile.

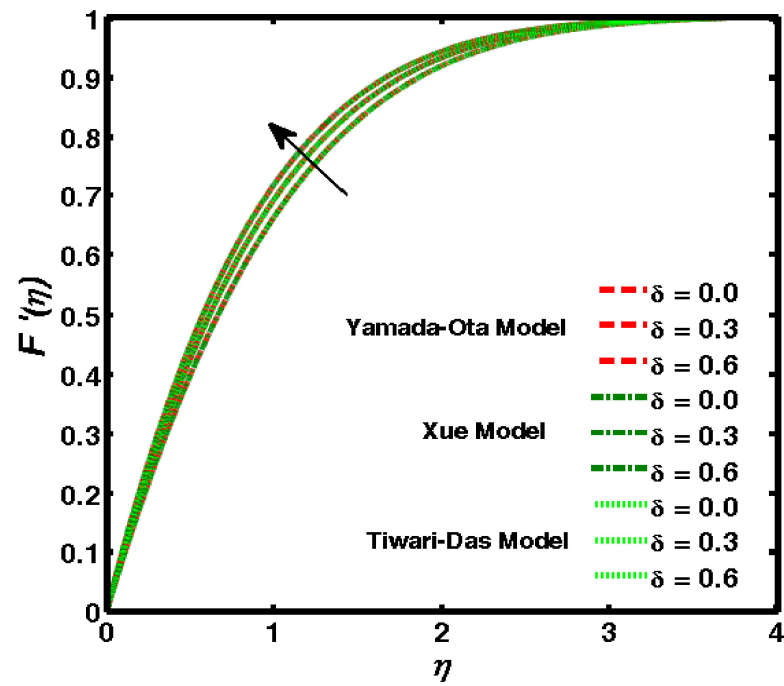**Figure 6.** Impacts of unsteadiness parameter on the velocity profile.

Figure 7. Impacts of magnetic field parameter on the velocity profile.
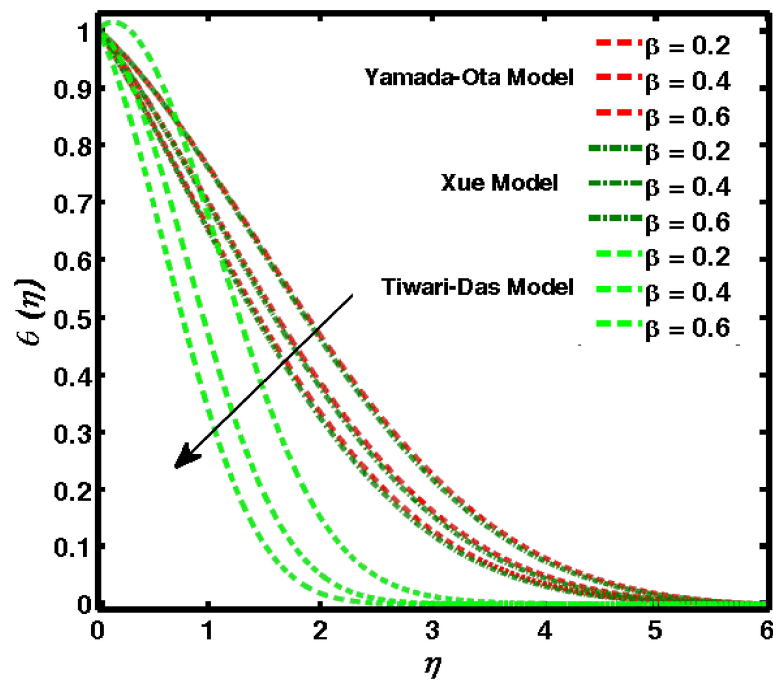

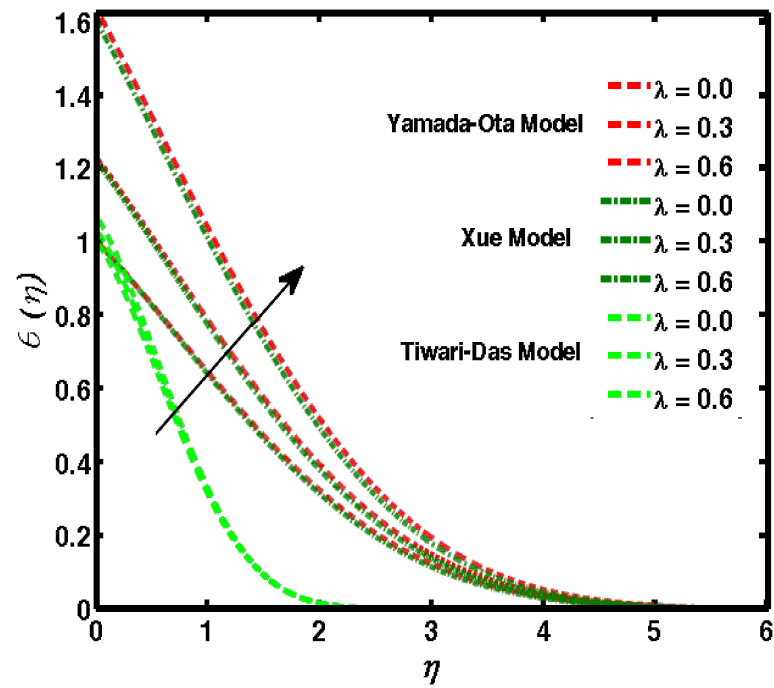**Figure 8.** Impacts of Casson fluid parameter on the temperature profile.

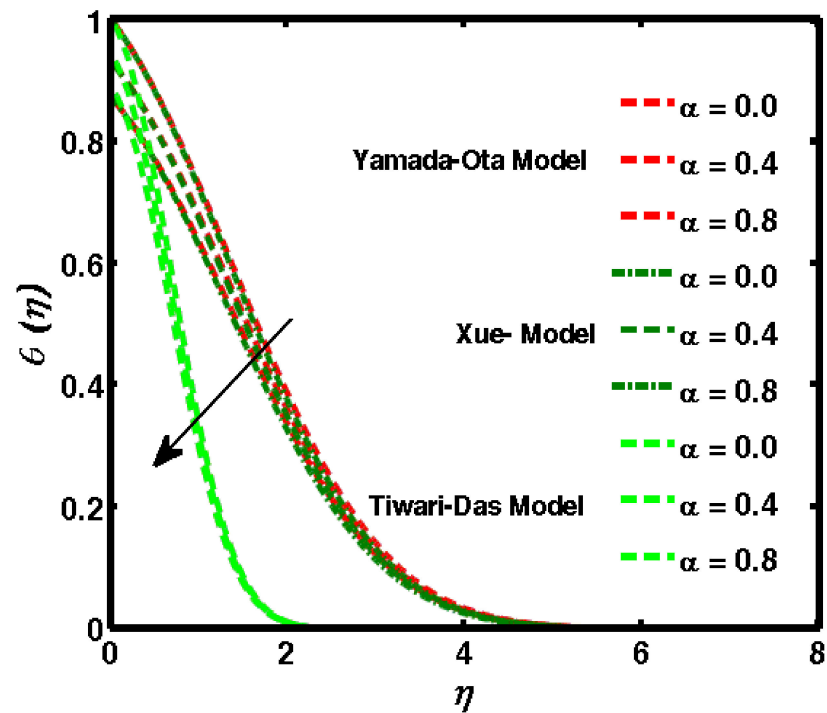**Figure 9.** Impacts of thermal slip on the temperature profile.

Figure 10. Impacts of unsteadiness parameter on the temperature profile.
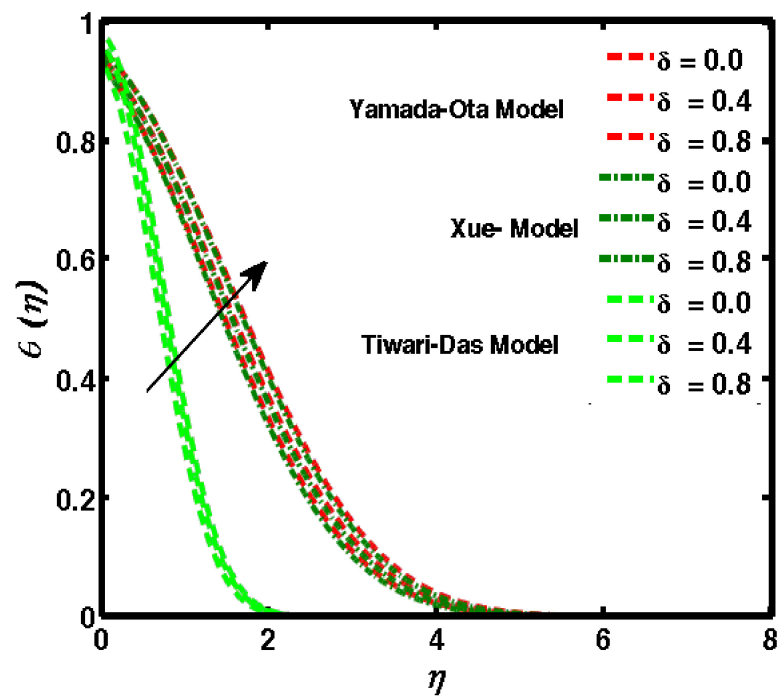
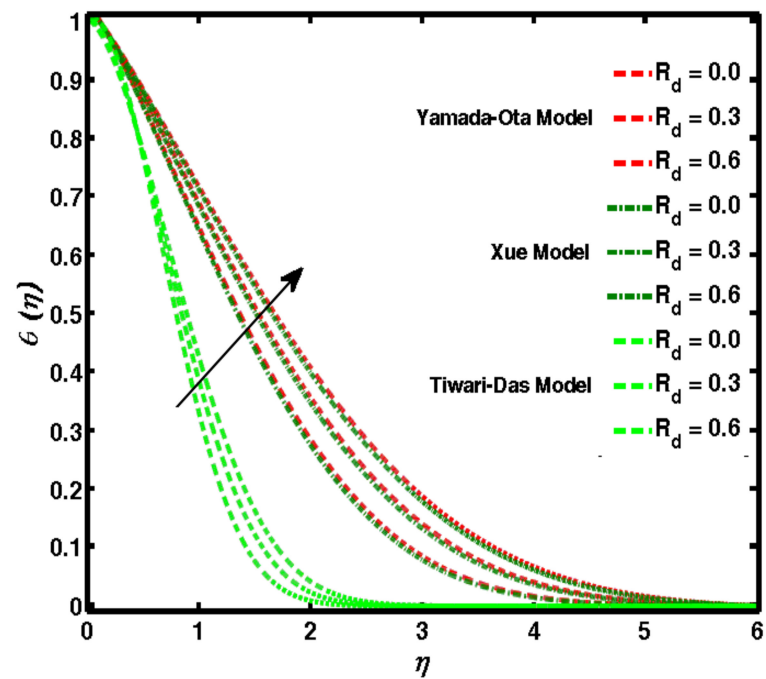**Figure 11.** Impacts of magnetic field parameter on the temperature profile.

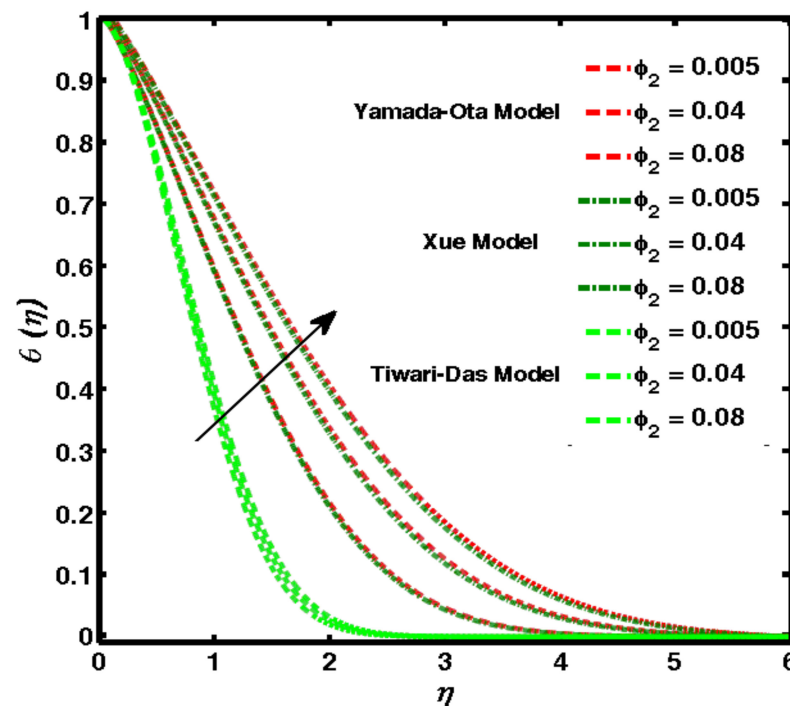**Figure 12.** Impacts of radiation parameter on the temperature profile.

Figure 13. Impacts of solid nanoparticle concentration on the temperature profile.

The impacts of physical parameters namely: unsteadiness parameter (α), solid nanoparticle concentration (ϕ_2), Casson fluid parameter (β), magnetic field parameter (δ), bouncy force parameter (τ), nonlinear radiation parameter (R_d) and thermal slip (λ) on the magnitude of temperature gradient ($Nu_x Re^{-1/2}$) and skin friction ($C_{fx} Re^{-1/2}$) presented through Table 1. The variation of unsteadiness parameter (α) and temperature gradient ($Nu_x Re^{-1/2}$) and skin friction ($C_{fx} Re^{-1/2}$) are revealed in Table 1. It is seen that skin friction ($C_{fx} Re^{-1/2}$) reduced while temperature gradient ($Nu_x Re^{-1/2}$) increased due to increment of unsteadiness parameter (α). The unsteadiness parameter depends on buoyancy and the influence of buoyancy is strong, so the flow is upward which reduced the skin friction. Table 1 indicated the impacts of solid nanoparticle concentration (ϕ_2) on temperature gradient ($Nu_x Re^{-1/2}$) and skin friction ($C_{fx} Re^{-1/2}$). It is seen that skin friction ($C_{fx} Re^{-1/2}$) increased and temperature gradient ($Nu_x Re^{-1/2}$) declined due to increment of solid nanoparticle concentration (ϕ_2). Physically, skin friction increased because higher values of the solid nanoparticles, increased resistance to the fluid motion. Table 1 indicated the impressions of the Casson fluid parameter (β) on the temperature gradient ($Nu_x Re^{-1/2}$) and skin friction ($C_{fx} Re^{-1/2}$). It is seen that skin friction ($C_{fx} Re^{-1/2}$) declined and temperature gradient ($Nu_x Re^{-1/2}$) increased due to the increment of Casson fluid parameter (β). Table 1 indicated the variation of magnetic field parameter (δ) and temperature gradient ($Nu_x Re^{-1/2}$) and skin friction ($C_{fx} Re^{-1/2}$). It is seen that skin friction ($C_{fx} Re^{-1/2}$) increased and temperature gradient ($Nu_x Re^{-1/2}$) declined due to increment of magnetic field parameter (δ). Table 1 indicated the variation of bouncy force parameter (τ) and temperature gradient ($Nu_x Re^{-1/2}$) and skin friction ($C_{fx} Re^{-1/2}$). It is seen that skin friction ($C_{fx} Re^{-1/2}$) increased but the temperature gradient ($Nu_x Re^{-1/2}$) also increased due to the increment of bouncy force parameter (τ) because the temperature buoyancy increased which leads to an increase in the skin friction and Nusselt number. Table 1 indicated the variation of the nonlinear radiation parameter (R_d) and temperature gradient ($Nu_x Re^{-1/2}$) and skin friction ($C_{fx} Re^{-1/2}$). It is seen that skin friction ($C_{fx} Re^{-1/2}$) reduced and temperature gradient ($Nu_x Re^{-1/2}$) increased due to increment of nonlinear radiation parameter (R_d). As the radiation increased which increased the heat transfer rate ultimately, the temperature gradient increased because of greater radiative structures characteristic of higher Nusselt numbers and much less thermal

irreversibilities. Table 1 indicated the variation of thermal slip (λ) and temperature gradient ($Nu_x Re^{-1/2}$) and skin friction ($C_{fx} Re^{-1/2}$). It is seen that skin friction ($C_{fx} Re^{-1/2}$) and temperature gradient ($Nu_x Re^{-1/2}$) increased due to increment of thermal slip (λ). Table 2 shows the comparative results of Wang [38] and Bachok et al. [39] with present results when the rest of the physical parameters are zero. It was found to be in good agreement with decay results.

Table 1. Numerical results of Nusselt Number and skin friction for different physical parameters.

Physical Parameters							Yamada−Ota Model		Xue Model		Tiwari−Das Model	
α	Φ_2	β	δ	τ	R_d	λ	$C_{fx}Re^{-1/2}$	$Nu_xRe^{-1/2}$	$C_{fx}Re^{-1/2}$	$Nu_xRe^{-1/2}$	$C_{fx}Re^{-1/2}$	$Nu_xRe^{-1/2}$
0.0	0.04	0.2	0.3	0.4	0.3	0.1	2.813517	0.064449	3.201124	0.06349211	2.952714	0.3956732
0.1	-	-	-	-	-	-	2.787466	0.068066	3.174606	0.06706521	2.94213	0.4376753
0.2	-	-	-	-	-	-	2.762156	0.07180177	3.148938	0.0707445	2.910595	0.4808478
0.3	-	-	-	-	-	-	2.737585	0.07566124	3.124121	0.07453456	2.880131	0.5236461
0.1	0.005	-	-	-	-	-	2.471826	0.131037	2.724885	0.1291255	2.62251	0.4898163
-	0.02	-	-	-	-	-	2.61435	0.09045102	2.910737	0.09189513	2.754804	0.4682181
-	0.04	-	-	-	-	-	2.813517	0.064449	3.174606	0.06706521	2.94213	0.4376753
-	0.06	-	-	-	-	-	3.026112	0.0511425	3.464069	0.05403433	3.1396	0.4104443
-	0.04	0.1	-	-	-	-	4.767978	0.04864135	5.241534	0.04724491	4.986934	0.1545644
-	-	0.2	-	-	-	-	3.577552	0.05691918	3.988893	0.05771476	3.74122	0.3087939
-	-	0.3	-	-	-	-	3.089422	0.06148109	3.469644	0.06339232	3.234315	0.388141
-	-	0.4	-	-	-	-	2.813517	0.064449	3.174606	0.06706521	2.94213	0.4376753
-	-	0.4	0.0	-	-	-	2.687217	0.0715124	3.014848	0.0777291	2.735188	0.7980804
-	-	-	0.1	-	-	-	2.751091	0.06793449	3.069072	0.07410157	2.806276	0.6741822
-	-	-	0.2	-	-	-	2.813517	0.064449	3.122306	0.07054838	2.875193	0.5541646
-	-	-	0.3	-	-	-	2.874588	0.06104927	3.174606	0.06706521	2.94213	0.4376753
-	-	-	0.3	0.1	-	-	2.874588	0.06104927	2.719003	0.06171291	2.719003	0.406732
-	-	-	-	0.2	-	-	3.030551	0.06280768	2.870635	0.06353266	2.794193	0.4173458
-	-	-	-	0.3	-	-	3.186904	0.06453459	3.022497	0.06531596	2.868553	0.4276537
-	-	-	-	0.4	-	-	3.343658	0.06623203	3.174606	0.06706521	2.94213	0.4376753
-	-	-	-	0.3	0.0	-	3.195023	0.05628139	3.179911	0.0580914	2.929671	0.3019853
-	-	-	-	-	0.1	-	3.191362	0.05909484	3.177421	0.06117104	2.934200	0.3490249
-	-	-	-	-	0.2	-	3.186904	0.06453459	3.175746	0.06415904	2.93833	0.3941719
-	-	-	-	-	0.3	-	3.185521	0.06717115	3.174606	0.06706521	2.94213	0.4376753
-	-	-	-	-	0.3	0.0	3.017863	0.03731803	3.01565	0.03958416	2.929241	0.3856542
-	-	-	-	-	-	0.1	3.186904	0.06453459	3.174606	0.06706521	2.94213	0.4376753
-	-	-	-	-	-	0.2	3.388235	0.1307413	4.45698	0.3207012	2.96317	0.5063074
-	-	-	-	-	-	0.3	3.593576	0.1636163	3.206887	0.4635417	2.985742	0.6004818

Table 2. Comparative results of Wang [38] and Bachok et al. [39] with existent outcomes when the rest of the physical parameters are zero.

$\in$	Wang [38]	Bachok et al. [39]	Present Results
0.0	1.232588	1.232588	1.231534
0.5	0.71330	0.713295	0.712761
1.0	0.0	0.0	0.0
2.0	−1.88731	−1.887307	−1.885872

4. Conclusions

The magnetic hydrodynamics time-dependent flow of Casson hybrid nanofluid at vertical stretching sheet is considered. The influence of the stagnation point region under the viscous dissipation and nonlinear electrically Lorentz forces are discussed. The system of differential equations is solved through numerical technique. The main results are presented below:

- The temperature function ($\theta(\eta)$) revealed to be declining due to improving the value of thermal slip (λ). Physically, the increment in thermal slip declined the surface drag leading to a decline in the production of heat amount which reduced the temperature distribution.
- The skin friction ($C_{fx}Re^{-1/2}$) and magnitude of temperature gradient ($Nu_xRe^{-1/2}$) declined due to increment of thermal slip (λ).
- The skin friction ($C_{fx}Re^{-1/2}$) increased and temperature gradient ($Nu_xRe^{-1/2}$) declined due to increment of solid nanoparticle concentration (ϕ_2). Physically, skin friction increased because of higher values of the solid nanoparticles, which increased resistance to the fluid motion.
- The curves of the temperature function ($\theta(\eta)$) revealed declining due to improving the value of Casson fluid parameter (β).
- The values of the nonlinear radiation parameter (R_d) increased which enhanced the curves of temperature function ($\theta(\eta)$) due
- The skin friction ($C_{fx}Re^{-1/2}$) and magnitude of temperature gradient ($Nu_xRe^{-1/2}$) declined due to increment of magnetic field parameter (δ).
- Yamada-Ota model of hybrid nanofluid achieved higher values as compared to Tiwari Das and Xue models of hybrid nanofluid.

Author Contributions: N.A. wrote the manuscript under the supervision of W.S. K.A. helped in the developing the results numerically and also helped in revised version. All authors have read and agreed to the published version of the manuscript.

Informed Consent Statement: Not applicable.

Data Availability Statement: Not applicable.

Conflicts of Interest: The authors declare no conflict of interest.

Nomenclature

v_{hnf}	Kinematic viscosity hybrid nanofluid
$k^*_{s_1}$ (SWCNT)	Thermal conductivity of solid nanoparticle
$k^*_{s_2}$ (MWCNT)	Thermal conductivity of solid nanoparticle
u, v	Velocity components
a	Stretching rate
v_f	Kinematic viscosity fluid
u_e	Free stream velocity
$\theta(\eta)$	Temperature function
$F(\eta)$	Velocity function
T_w	Wall temeparature
T_∞	Ambient temperature
ϕ_1 (SWCNT)	Solid nanopartcile concentration
β	Casson fluid parameter
ϕ_2 (MWCNT)	Solid nanopartcile concentration
$(c_P)_{s_1}$ (SWCNT)	Heat capacity of solid nanoparticle
ρ_{s_2} (MWCNT)	Density of solid nanoparticle
K_{hnf}	Thermal conductivity of hybrid nanofluid
λ	Thermal slip
Pr	Prandtle number
α	Unsteadyness parameter
ρ_f	Density of fluid
$(c_P)_{s_2}$ (MWCNT)	Heat capacity of solid nanoparticle
$(c_P)_f$	Heat capacity of fluid
ρ_{s_1} (SWCNT)	Density of solid nanoparticle
k^*_f	Thermal conductivity of fluid
R_d	Radiation parameter
τ	Bouncy forces
δ	Magnetic field

References

1. Choi, S.U.; Eastman, J.A. *Enhancing Thermal Conductivity of Fluids with Nanoparticles*; No. ANL/MSD/CP-84938; CONF-951135-29; Argonne National Lab. (ANL): Argonne, IL, USA, 1995.
2. Reddy, N.N.; Rao, V.S.; Reddy, B.R. Impact of thermal radiation and chemical reaction on MHD heat and mass transfer Casson nanofluid flow past a stretching sheet in presence of heat source/sink. *ARPN J. Eng. Appl. Sci.* **2006**, *16*, 1165–1172.
3. Vajravelu, K.; Prasad, K.V.; Lee, J.; Lee, C.; Pop, I.; Van Gorder, R.A. Convective heat transfer in the flow of viscous Ag–water and Cu–water nanofluids over a stretching surface. *Int. J. Therm. Sci.* **2011**, *50*, 843–851. [CrossRef]
4. Suresh, S.; Venkitaraj, K.P.; Selvakumar, P.; Chandrasekar, M. Effect of Al₂O₃–Cu/water hybrid nanofluid in heat transfer. *Exp. Therm. Fluid Sci.* **2012**, *38*, 54–60. [CrossRef]
5. Suresh, S.; Venkitaraj, K.P.; Hameed, M.S.; Sarangan, J. Turbulent heat transfer and pressure drop characteristics of dilute water based Al₂O₃–Cu hybrid nanofluids. *J. Nanosci. Nanotechnol.* **2014**, *14*, 2563–2572. [CrossRef]
6. Takabi, B.; Shokouhmand, H. Effects of Al₂O₃–Cu/water hybrid nanofluid on heat transfer and flow characteristics in turbulent regime. *Int. J. Mod. Phys. C* **2015**, *26*, 1550047. [CrossRef]
7. Nadeem, S.; Abbas, N.; Khan, A.U. Characteristics of three dimensional stagnation point flow of Hybrid nanofluid past a circular cylinder. *Results Phys.* **2018**, *8*, 829–835. [CrossRef]
8. Nadeem, S.; Abbas, N. On both MHD and slip effect in micropolar hybrid nanofluid past a circular cylinder under stagnation point region. *Can. J. Phys.* **2019**, *97*, 392–399. [CrossRef]
9. Nadeem, S.; Abbas, N.; Malik, M.Y. Inspection of hybrid based nanofluid flow over a curved surface. *Comput. Methods Programs Biomed.* **2020**, *189*, 105193. [CrossRef]
10. Abbas, N.; Nadeem, S.; Saleem, A.; Malik, M.Y.; Issakhov, A.; Alharbi, F.M. Models base study of inclined MHD of hybrid nanofluid flow over nonlinear stretching cylinder. *Chin. J. Phys.* **2021**, *69*, 109–117. [CrossRef]
11. Abbas, N.; Rehman, K.U.; Shatanawi, W.; Malik, M.Y. Numerical study of heat transfer in hybrid nanofluid flow over permeable nonlinear stretching curved surface with thermal slip. *Int. Commun. Heat Mass Transf.* **2022**, *135*, 106107. [CrossRef]
12. Li, P.; Duraihem, F.Z.; Awan, A.U.; Al-Zubaidi, A.; Abbas, N.; Ahmad, D. Heat Transfer of Hybrid Nanomaterials Base Maxwell Micropolar Fluid Flow over an Exponentially Stretching Surface. *Nanomaterials* **2022**, *12*, 1207. [CrossRef] [PubMed]

13. Neethu, T.S.; Sabu, A.S.; Mathew, A.; Wakif, A.; Areekara, S. Multiple linear regression on bioconvective MHD hybrid nanofluid flow past an exponential stretching sheet with radiation and dissipation effects. *Int. Commun. Heat Mass Transf.* **2022**, *135*, 106115. [CrossRef]

14. Casson, N. A Flow Equation for Pigment-Oil Suspensions of the Printing Ink Type. In *Rheology of Disperse Systems*; Pergamon Press: Oxford, UK, 1959.

15. Abbas, N.; Shatanawi, W. Heat and Mass Transfer of Micropolar-Casson Nanofluid over Vertical Variable Stretching Riga Sheet. *Energies* **2022**, *15*, 4945. [CrossRef]

16. Nadeem, S.; Haq, R.U.; Akbar, N.S. MHD three-dimensional boundary layer flow of Casson nanofluid past a linearly stretching sheet with convective boundary condition. *IEEE Trans. Nanotechnol.* **2013**, *13*, 109–115. [CrossRef]

17. Oyelakin, I.S.; Mondal, S.; Sibanda, P. Unsteady Casson nanofluid flow over a stretching sheet with thermal radiation, convective and slip boundary conditions. *Alex. Eng. J.* **2016**, *55*, 1025–1035. [CrossRef]

18. Ibrahim, S.M.; Lorenzini, G.; Kumar, P.V.; Raju, C.S.K. Influence of chemical reaction and heat source on dissipative MHD mixed convection flow of a Casson nanofluid over a nonlinear permeable stretching sheet. *Int. J. Heat Mass Transf.* **2017**, *111*, 346–355. [CrossRef]

19. Amjad, M.; Zehra, I.; Nadeem, S.; Abbas, N.; Saleem, A.; Issakhov, A. Influence of Lorentz force and induced magnetic field effects on Casson micropolar nanofluid flow over a permeable curved stretching/shrinking surface under the stagnation region. *Surf. Interfaces* **2020**, *21*, 100766. [CrossRef]

20. Lanjwani, H.B.; Saleem, S.; Chandio, M.S.; Anwar, M.I.; Abbas, N. Stability analysis of triple solutions of Casson nanofluid past on a vertical exponentially stretching/shrinking sheet. *Adv. Mech. Eng.* **2021**, *13*, 16878140211059679. [CrossRef]

21. Tawade, J.V.; Guled, C.N.; Noeiaghdam, S.; Fernandez-Gamiz, U.; Govindan, V.; Balamuralitharan, S. Effects of thermophoresis and Brownian motion for thermal and chemically reacting Casson nanofluid flow over a linearly stretching sheet. *Results Eng.* **2022**, *15*, 100448. [CrossRef]

22. Abbas, Z.; Imran, M.; Naveed, M. Impact of Equally Diffusive Chemical Reaction on Time-Dependent Flow of Casson Nanofluid Due to Oscillatory Curved Stretching Surface with Thermal Radiation. *Arab. J. Sci. Eng.* **2022**, 1–20. Available online: https://link.springer.com/article/10.1007/s13369-022-06792-8 (accessed on 6 June 2022).

23. Ramzan, M.; Gul, H.; Malik, M.Y.; Ghazwani, H.A.S. Entropy Minimization Analysis of a Partially Ionized Casson Nanofluid Flow over a Bidirectional Stretching Sheet with Surface Catalyzed Reaction. *Arab. J. Sci. Eng.* **2022**, 1–13. Available online: https://link.springer.com/article/10.1007/s13369-021-06492-9 (accessed on 6 June 2022).

24. Yang, K.T. Unsteady laminar boundary layers in an incompressible stagnation flow. *J. Appl. Mech.* **1958**, *25*, 421–427. [CrossRef]

25. Wang, C.Y. Liquid film on an unsteady stretching surface. *Q. Appl. Math.* **1990**, *48*, 601–610. [CrossRef]

26. Abbas, Z.; Hayat, T.; Sajid, M.; Asghar, S. Unsteady flow of a second grade fluid film over an unsteady stretching sheet. *Math. Comput. Model.* **2008**, *48*, 518–526. [CrossRef]

27. Mabood, F.; Shateyi, S. Multiple slip effects on MHD unsteady flow heat and mass transfer impinging on permeable stretching sheet with radiation. *Model. Simul. Eng.* **2019**, *2019*, 3052790. [CrossRef]

28. Fuzhang, W.; Anwar, M.I.; Ali, M.; El-Shafay, A.S.; Abbas, N.; Ali, R. Inspections of unsteady micropolar nanofluid model over exponentially stretching curved surface with chemical reaction. *Waves Random Complex Media* **2022**, 1–22. [CrossRef]

29. Abbas, N.; Nadeem, S.; Khan, M.N. Numerical analysis of unsteady magnetized micropolar fluid flow over a curved surface. *J. Therm. Anal. Calorim.* **2022**, *147*, 6449–6459. [CrossRef]

30. Iqbal, Z.; Khan, M.; Shoaib, M.; Matoog, R.T.; Muhammad, T.; El-Zahar, E.R. Study of buoyancy effects in unsteady stagnation point flow of Maxwell nanofluid over a vertical stretching sheet in the presence of Joule heating. *Waves Random Complex Media* **2022**, 1–15. [CrossRef]

31. Yamada, E.; Ota, T. Effective thermal conductivity of dispersed materials. *Wärme-Und Stoffübertragung* **1980**, *13*, 27–37. [CrossRef]

32. Xue, Q.Z. Model for thermal conductivity of carbon nanotube-based composites. *Phys. B* **2005**, *368*, 302–307. [CrossRef]

33. Tiwari, R.K.; Das, M.K. Heat transfer augmentation in a two-sided lid-driven differentially heated square cavity utilizing nanofluids. *Int. J. Heat Mass Transf.* **2007**, *50*, 2002–2018. [CrossRef]

34. Abbas, N.; Nadeem, S.; Malik, M.Y. On extended version of Yamada–Ota and Xue models in micropolar fluid flow under the region of stagnation point. *Phys. A Stat. Mech. Its Appl.* **2020**, *542*, 123512. [CrossRef]

35. Abbas, N.; Malik, M.Y.; Nadeem, S.; Alarifi, I.M. On extended version of Yamada–Ota and Xue models of hybrid nanofluid on moving needle. *Eur. Phys. J. Plus* **2020**, *135*, 1–16. [CrossRef]

36. Zingg, D.W.; Chisholm, T.T. Runge–Kutta methods for linear ordinary differential equations. *Appl. Numer. Math.* **1999**, *31*, 227–238. [CrossRef]

37. Abbas, N.; Malik, M.Y.; Nadeem, S.; Hussain, S.; El-Shafa, A.S. Similarity solution of second grade fluid flow over a moving cylinder. *Int. J. Mod. Phys. B* **2021**, *35*, 2150325. [CrossRef]

38. Wang, C.Y. Stagnation flow towards a shrinking sheet. *Int. J. Non-Linear Mech.* **2008**, *43*, 377–382. [CrossRef]

39. Bachok, N.; Ishak, A.; Pop, I. Stagnation-point flow over a stretching/shrinking sheet in a nanofluid. *Nanoscale Res. Lett.* **2011**, *6*, 1–10. [CrossRef]